Analytical and Bioanalytical Chemistry
https://doi.org/10.1007/s00216-019-02314-y

RESEARCH PAPER

A highly sensitive electrochemical biosensor for protein based on a tetrahedral DNA probe, N- and P-co-doped graphene, and rolling circle amplification

Zhi-Wei Wu[1] · Xing-Chen Xie[1] · Hong-Ran Guo[2] · Huan Xia[1] · Ke-Jing Huang[1]

Received: 17 September 2019 / Revised: 24 November 2019 / Accepted: 2 December 2019

Abstract

A tetrahedral DNA probe can effectively overcome the steric effects of a single-stranded probe to obtain well-controlled density and minimize nonspecific adsorption. Herein, a highly sensitive electrochemical biosensor is fabricated for determination of protein using a tetrahedral DNA probe and rolling circle amplification (RCA). N- and P-co-doped graphene (NP-rGO) is prepared, and AuNPs are then electrodeposited on it for DNA probe immobilization. Benefitting from the synergistic effects of the excellent electrical conductivity of NP-rGO, the stability of the tetrahedral DNA probe and the signal amplification of RCA, the biosensor achieves a low limit of 3.53×10^{-14} M for thrombin and a wide linear range from 1×10^{-13} to 1×10^{-7} M. This study provides a sensitive and effective method for the detection of protein in peripheral biofluids, and paves the way for future clinical diagnostics and treatment of disease.

Keywords Tetrahedral DNA probe · N- and P-Co-doped graphene · Rolling circle amplification · Protein · Sensitive determination

Introduction

Protein is an essential component of organisms, and it participates in various important physiological processes. The research on its structure and function as well as qualitative and quantitative detection are of great significance in clinical diagnosis, disease treatment, drug screening and human health [1, 2]. However, it is still difficult to accurately detect proteins in biological samples due to their high molecular weight, complex structure and low abundance [3].

Aptamer has been widely used for improving the sensitivity of protein assays [4, 5], as it can recognize various kinds of targets with high selectivity [6], and many highly sensitive electrochemical biosensors have recently been prepared based on aptamer [7–10]. However, there are still some deficiencies in aptamer biosensors, such as the effect of density and orientation of aptamer on the electrode. Therefore, three-dimensional DNA probes have recently received increasing attention owing to their precise controllability along a designated path [11, 12]. The three-dimensional structure has a high DNA loading capacity and can significantly enhance the local effective level of the probe and the reaction efficiency [13, 14]. Most recently, a tetrahedral DNA nanostructure was prepared, and its stereo structure was able to exactly control the assembled DNA probe on the electrode interface and therefore enhance accessibility and reactivity, and prevent the entrance of spacer molecules [15, 16].

Charge transfer and surface active sites are both important properties which directly determine the performance of electrochemical biosensors. Using various functional materials to modify electrodes can effectively improve their active sites and electro-conductivity [17, 18]. Graphene has received increasing attention as an active electrode material owing to its distinctive properties, such as excellent electrical and mechanical properties, high specific surface area, and the feasibility of large-scale chemical fabrication of modified graphene [19, 20]. However, two-dimensional graphene nanosheets suffer from poor conductivity as a result of low quality or high junction contact resistance due to the π–π contacts [21, 22]. Therefore, doping graphene with heteroatoms is introduced

✉ Ke-Jing Huang
kejinghuang11@163.com

[1] College of Chemistry and Chemical Engineering, Xinyang Normal University, 237# Chang An Road, Xinyang 464000, Henan, China

[2] School of Chemistry and Chemical Technology, Shanghai Jiaotong University, Shanghai 200240, China

Published online: 03 January 2020

as a solution to prevent the restacking of the sheets [23]. Furthermore, graphene doped with heteroatoms (such as N, B, S and P) either singly or dually can improve its electrical conductivity and surface area [24]. Incorporation of heteroatoms in the graphene lattice is also helpful because it improves the charge density of states and wettability of the electrode for enhanced electrochemical performance [25, 26].

A variety of isothermal amplification techniques have recently been used to increase the sensitivity of protein analysis, such as rolling circle amplification (RCA) [27], helicase-dependent amplification [28], exonuclease-assisted signal amplification [29] and loop-mediated isothermal amplification [30]. In particular, RCA not only directly amplifies specific DNA and RNA molecules but also amplifies the signal of the targets. Most importantly, RCA can be carried out under mild conditions and does not require expensive equipment to circulate temperature. Therefore, RCA has been rapidly developed and applied to sensitively determine RNAs, proteins and drugs [31].

In this paper, an RCA signal amplification strategy coupled with the tetrahedral DNA probe for sensitive and highly specific detection of thrombin (TB) is developed using N- and P-co-doped graphene (NP-rGO) as electrode substrate. NP-rGO is first modified on the electrode, which not only improves the loading amount of the DNA probe but also accelerates the electron transfer due to its large specific surface area and excellent conductivity. The Au nanoparticles (AuNPs) are then electrodeposited on NP-rGO, and the three-dimensional DNA probe (T-DNA) is immobilized on the electrode by Au–S bonds. After modification with TB, the electrode undergoes an RCA reaction to obtain the biosensor. The biosensor combines the distinct recognition specificity of the tetrahedral DNA probe and the powerful signal amplification capability of RCA. The proposed biosensor employs N- and P-co-doped graphene to modify the electrode, providing more surface electrochemically active sites and faster charge transfer. The introduction of a tetrahedral DNA nanostructure in the biosensor results in a large DNA loading capacity and enhances the local effective level of the probe and the reaction efficiency. Therefore, this biosensor may represent a highly sensitive and selective platform for the detection of protein, and will be a very promising strategy in future clinical diagnostics and treatment of disease.

Experimental

Reagents and materials

Graphite powder, ethylene glycol, thiocarbamide, Tris(hydroxymethyl-1)aminomethane (Tris), Tris(2-carboxyethyl)phosphine hydrochloride (TCEP), H_2O_2, $HAuCl_4$, immunoglobin G (IgG), prostate-specific antigen (PSA), hemoglobin (Hb), $MgCl_2$, $(NH_4)_2SO_4$ and hydroquinone (HQ) were purchased from Shanghai Xueman Biotechnology Co., Ltd. (China). Phi 29 DNA polymerase, T DNA ligase, deoxyribonucleoside 5′-triphosphates mixtures (dNTPs), thrombin (TB) and 6-mercaptohexanol (MCH) were obtained from Aladdin Chemicals Co. Ltd. (Shanghai, China). The DNA sequences (Table 1) were acquired from Shanghai Sangon Biological Engineering Technology Co., Ltd. (Shanghai, China) [7, 32].

Instrumentation

Electrochemical tests were conducted on an RST5200F electrochemical workstation (Zhengzhou Shi Rui Si Instrument, Zhengzhou, China). A modified glassy carbon electrode (GCE), Ag/AgCl electrode and platinum wire were used as the working electrode, the reference electrode and auxiliary electrode, respectively. The chemical composition of the samples was examined using X-ray photoelectron spectroscopy (XPS, K-Alpha 0.5 eV, Thermo Fisher Scientific, MA, USA) and energy-dispersive X-ray spectroscopy (EDS). The morphology and structure were observed by transmission electron microscopy (TEM, Hitachi H800) and scanning electron microscopy (SEM, JEOL JSM-6510). The crystalline properties and phase were determined by X-ray powder diffraction (XRD) using a Rigaku diffractometer (Rigaku, Tokyo, Japan). To analyze the defects and purity, an RM 1000 Raman spectrometer (Renishaw, Gloucestershire, UK) was used.

Synthesis of nanomaterials

N- and P-co-doped graphene was synthesized as follows: First, graphene oxide (GO) was prepared according to a reported assay [33]. The NP-rGO was then prepared [34]. Briefly, 50 mg GO and 15 mg $(NH_4)_2HPO_4$ were added to 50 mL water. The mixture was stirred for 1 h, and the water was then removed. Next, the mixture was heated under N_2 at 900 °C for 60 min, after which the sample was cooled and washed with water and ethanol, and dried overnight in vacuum at 60 °C.

Fabrication of the biosensor

The T-DNA was synthesized as follows: Four single-stranded DNAs (tetrahedron a, b, c, d) were dissolved separately in 10 mM Tris-HCl buffer solution (pH 8.0) containing 10 mM TCEP and 10 mM $MgCl_2$ to obtain 4 μM solutions. Then, four equal-volume solutions were mixed and incubated at 95 °C for 2 min.

Bare GCEs were burnished using different particle sizes of Al_2O_3 slurries. After ultrasonic cleaning by ethanol solution, they were washed again with DI water. Subsequently, 8 μL NP-rGO (1 mg/mL) was applied on the electrode, and then kept in 0.1% $HAuCl_4$ for electrodeposition of AuNPs at −0.2 V for

Table 1 DNA sequences used in this work

Note	Sequence (5′–3′)
Tetrahedron a	ACATTCCTAAGTCTGAAACATTACAGCTTGCTACACGAGAAGAGCCGCCATAGTATTTTTTTTTTGTAGGGCAGG
Tetrahedron b	SH-C6-TATCACCAGGCAGTTGACAGTGTAGCAAGCTGTAATAGATGCGAGGGTCCAATAC
Tetrahedron c	SH-C6-TCAACTGCCTGGTGATAAAACGACACTACGTGGGAATCTACTATGGCGGCTCTTC
Tetrahedron d	SH-C6-TTCAGACTTAGGAATGTGCTTCCCACGTAGTGTCGTTTGTATTGGACCCTCGCAT
Aptamer	AGTCCGTGGTAGGGCAGGTTGGGGTGACTTTTT
cDNA1	GTCACCCCAACCTGCCCTTT
cDNA2	GTCACCCCAACCTGCCCTACTTT
cDNA3	GTCACCCCAACCTGCCCTACCACTTT
Primer probe	TTGGGGTGACATCCCTATAAATACCCTAAC
Loop probe	Phosphate-TTATAGGGTATCTCTATCTCTTAGGGTAT
Signal probe (SP)	5′-Biotin-TATCTCTATCTC-3’

60 s. Next, 8 μL T-DNA (1 μM) was applied on the AuNPs/NP-GrO/GCE and kept at 4 °C overnight. The electrode was then dipped in 5 μL MCH (0.5 mM) and incubated for 1 h.

Five milliliters TB and 2 μL aptamer (0.5 μM) were then mixed at 30 °C and shaken for 2 h. Two milliliters cDNA (0.5 μM) was added to the above mixture and maintained at 30 °C for 60 min. It was subsequently applied on the modified electrode and kept at 30 °C for 60 min. The electrode was then immersed in primer probe solution (1 μM) for 1 h, after which it was dipped in Tris-HCl buffer with 1 μM loop probe, 5 unit/mL T-DNA ligase, 10 mM $MgCl_2$, 10 mM dithiothreitol (DTT) and 1 mM adenosine triphosphate at 22 °C for 60 min. The linear loop probe was hybridized with the primer probe, and the nick created was linked by T-DNA ligase. This electrode was then dipped in 50 mmol/L Tris-HCl solution containing 10 nmol/L $(NH_4)_2SO_4$, 10 nmol/L $MgCl_2$, 4 mM DTT, 0.2 mg/mL bovine serum albumin (BSA), 0.5 mM deoxynucleotide polymerase and 50 unit/mL phi29 DNA polymerase at 37 °C for 60 min to produce long ssDNA. Eight milliliters of SP was then added and incubated for 1 h. Finally, 8 μL avidin-horseradish peroxidase (HRP) (10 μg/mL) was applied on the electrode and incubated for 0.5 h. The mechanism involved in the fabrication process is exhibited in Scheme 1.

Results and discussion

Characterization of N- and P-co-doped graphene

The morphology of NP-rGO was detected with TEM and SEM. Figure 1a shows an ultrathin layered nanostructure of NP-rGO. The nanosheets provide not only large specific surface area but also rich active edges for constructing a sensitive sensing platform. The TEM image in Fig. 1b again exhibits the ultrathin nanosheets of NP-rGO.

The elemental composition of the NP-rGO was studied by EDS analysis (Fig. 1c). The results show that the NP-rGO is composed of C, O, N and P. The C atom is the main component, and N is 4% of the composite.

The XPS spectrum in Fig. 1d confirms that the NP-rGO is composed of C, O, N and P. In Fig. 1e, the peaks at 133.6 (P–C) and 134.3 eV (P–O) are consistent with the characteristic peak of P 2p. In Fig. 1f, the high resolution of the N 1s band shows four forms of N (oxidized N, pyridinic N, pyrrolic N and graphitic N) in the sample at 399.2, 400.9, 401.6 and 402.4 eV, respectively.

Electrochemical characterization

TThe step-by-step assembly process of the biosensor was studied by cyclic voltammetry (CV) (Fig. 2A and B). Two redox peaks (curve a) appear on the bare GCE, while the redox peak currents obviously increase after NP-rGO is modified on the GCE (curve b) due to its good conductivity. When AuNPs are deposited on the NP-rGO/GCE, one large peak current is obtained (curve c). This may have benefited from the facilitated

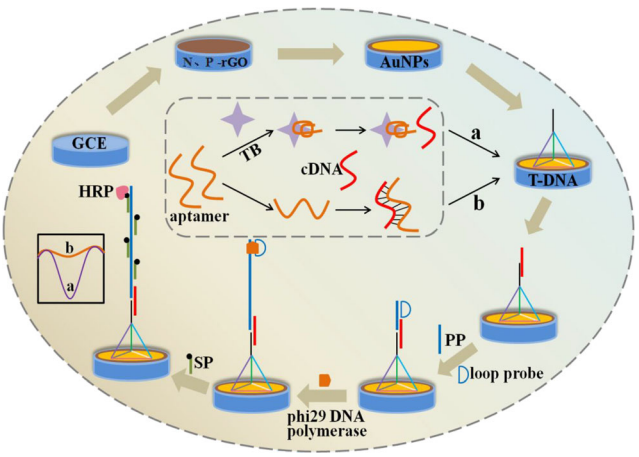

Scheme 1 Preparation of the thrombin biosensor

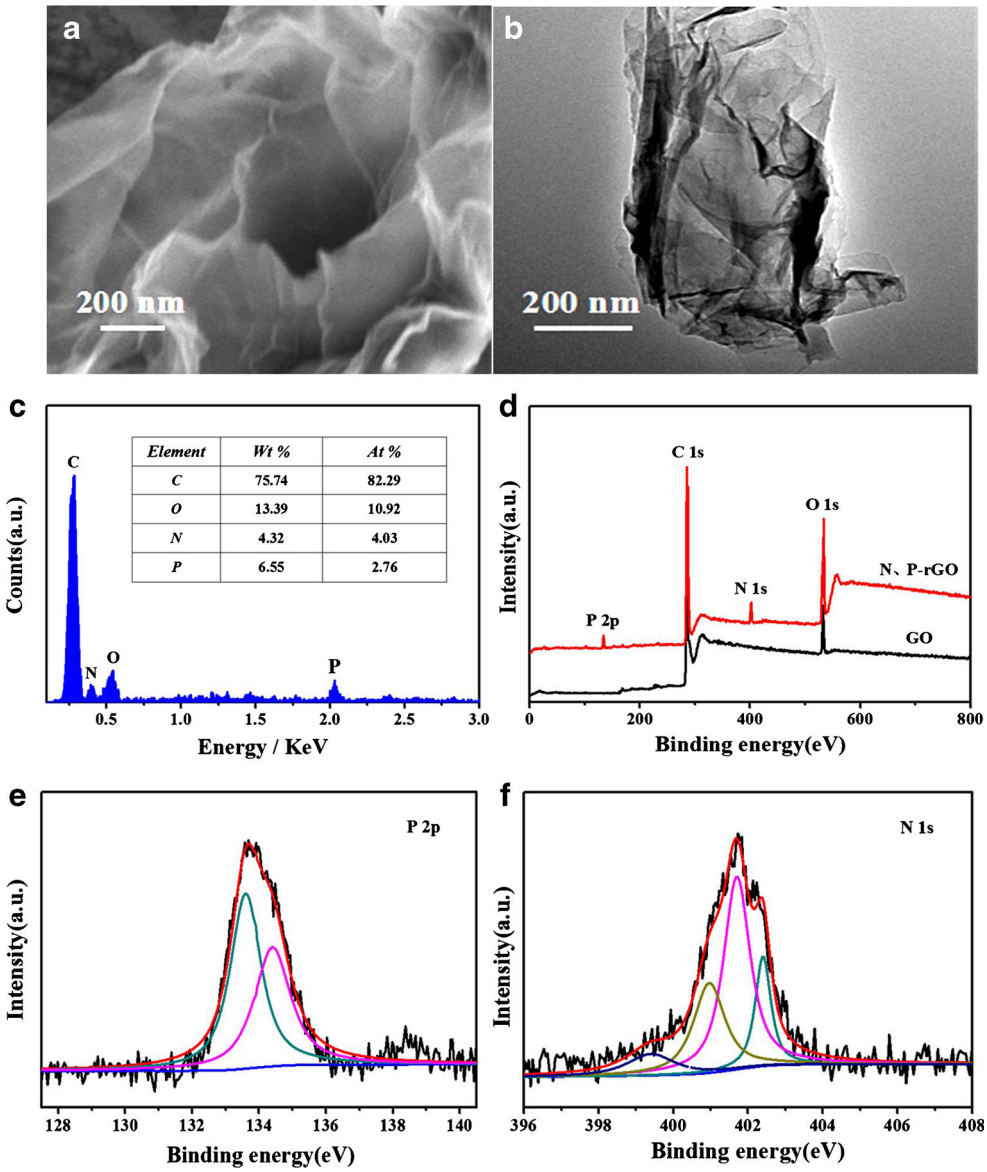

Fig. 1 SEM (**a**), TEM (**b**), EDS (**c**) and XPS spectrum (**d**) of NP-rGO; high-resolution XPS spectra of P 2p (**e**) and N 1s (**f**) of NP-rGO

electron transfer provided by AuNPs. However, after T-DNA and cDNA were fixed on the electrode and RCA occurred, the current response gradually decreased due to negatively charged DNA which makes electron transfer more difficult (curves d–h).

Electrochemical impedance spectroscopy (EIS) was also used to determine the preparation process of the modified electrode. AuNPs/NP-rGO/GCE (curve c) displays the smallest semicircle and electron transfer resistance (R_{et}) (Fig. 2C), suggesting the AuNPs/NP-rGO film promotes electron transfer. Then, the R_{et} is increasingly enhanced with the sequential immobilizing of T-DNA (curve d), cDNA (curve e), PP + loop probe (curve f), RCA product (curve g) and SP (curve h) on AuNPs/NP-rGO (Fig. 2D). This phenomenon demonstrates successful preparation of the biosensor.

Figure 2E shows the differential pulse voltammetry (DPV) of different electrodes. The DPV current signal of NP-rGO/GCE is greatly improved compared with bare GCE, due to its good conductivity. After AuNPs are further modified on the NP-rGO/GCE, the current signal obviously increases. When T-DNA, cDNA, PP + loop probe, RCA products and SP are gradually immobilized on the AuNPs/NP-rGO/GCE, the DPV signals decrease step by step, confirming successful preparation of the biosensor. Figure 2F shows the EIS of P-rGO/GCE, N-rGO/GCE and NP-rGO/GCE. The results reveal that the NP-rGO/GCE has the lowest R_{et} value, indicating good conductivity.

Optimization

The effect of deposition time of AuNPs on the DPV signal was evaluated from 10 to 120 s (Fig. 3a). The DPV signal is increased with increasing deposition time, and then remains

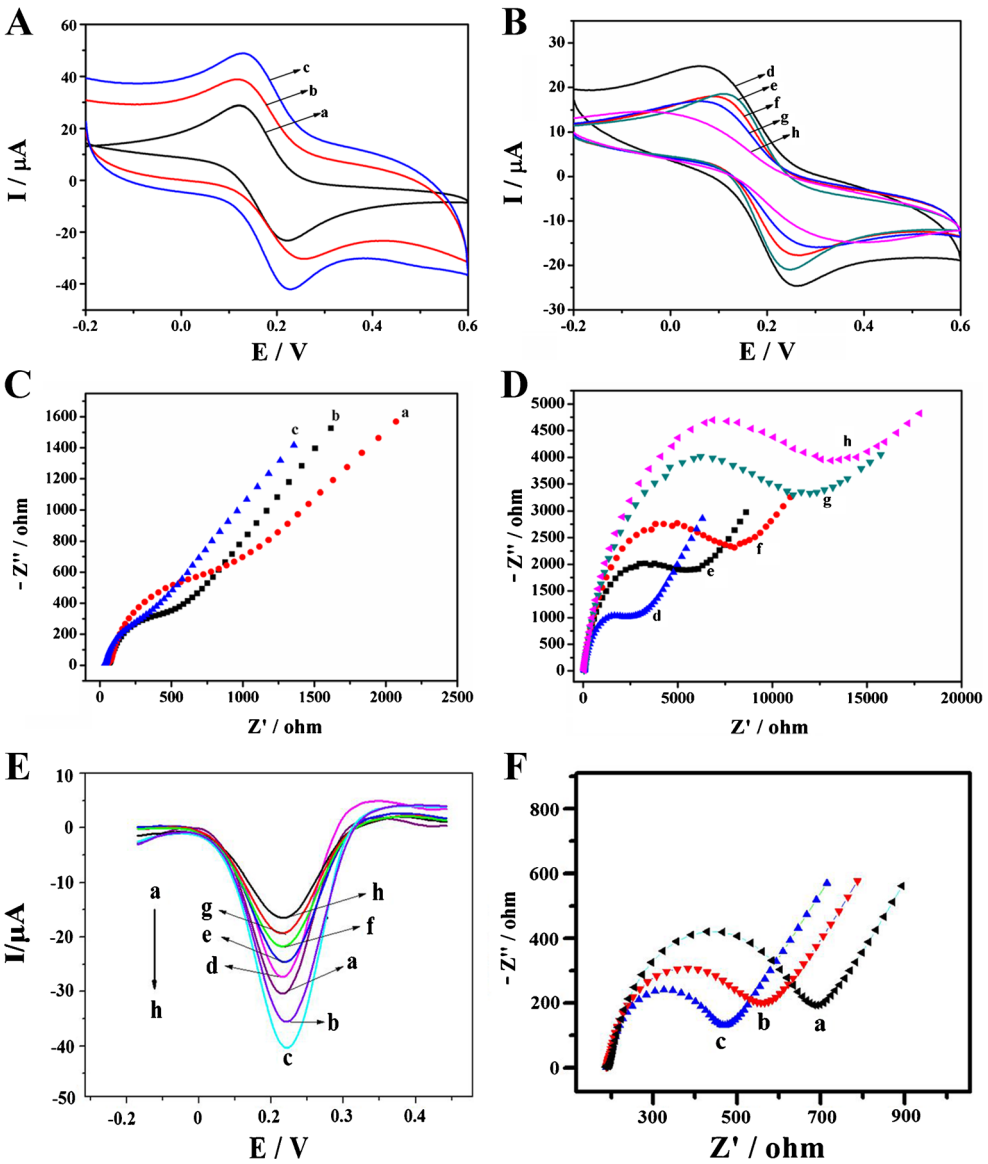

Fig. 2 CV curves (**A**, **B**), EIS (**C**, **D**) and DPV (**E**) of different electrodes: (**a**) GCE, (**b**) NP-rGO/GCE, (**c**) AuNPs/NP-rGO/GCE, (**d**) T-DNA/AuNPs/NP-rGO/GCE, (**e**) cDNA/T-DNA/AuNPs/NP-rGO/GCE, (**f**) PP + loop probe/cDNA/T-DNA/AuNPs/NP-rGO/GCE, (**g**) RCA/PP + loop probe/cDNA/T-DNA/AuNPs/NP-rGO/GCE, (**h**) SP/RCA/PP + loop probe/cDNA/T-DNA/AuNPs/NP-rGO/GCE; (**F**) EIS of P-rGO/GCE (**a**), N-rGO/GCE (**b**) and NP-rGO/GCE (**c**)

unchanged after 1 min, suggesting an appropriate amount of AuNPs was deposited on the electrode.

The effect of the pH of the electrolyte was studied. Figure 3b shows that the largest current signal is achieved with a pH value of 7.0. Consequently, pH 7.0 was chosen in this experiment.

The effect of the sequence length of cDNA was also evaluated (Fig. 3c). Three cDNAs (cDNA1, cDNA2, cDNA3) with 20, 23 and 26 base numbers were applied, which were partly complementary with aptamer. When cDNA2 was used, the highest DPV response was obtained. This is because the short DNA chain cannot preferably fix with the vertical domain of T-DNA, and the long DNA chain can hybridize with aptamer.

Some RCA conditions were also optimized. The effect of different concentrations of T-DNA ligase (1, 2, 3, 4, 5, 6 and 7 unit/mL) was evaluated. The results show that an increase in the concentration of ligase from 1 to 5 unit/mL results in a gradual increase in signal intensity. However, when the concentration continues to increase beyond 5 unit/mL, the signal intensity remains almost unchanged. Therefore, 5 unit/mL of T-DNA ligase was used.

The effect of various concentrations of Phi29 DNA polymerase was investigated. The results show that as the concentration of Phi29 DNA polymerase is increased from 10 to 80 unit/mL, the current signal intensity demonstrates a gradual increase until the concentration of Phi29 DNA polymerase reaches 50 unit/mL, after which the signal intensity decreases. Therefore, 50 unit/mL was chosen.

Analytical performance

TB solutions of various concentrations were detected with the biosensor (Fig. 4A). A linear relationship between the DPV

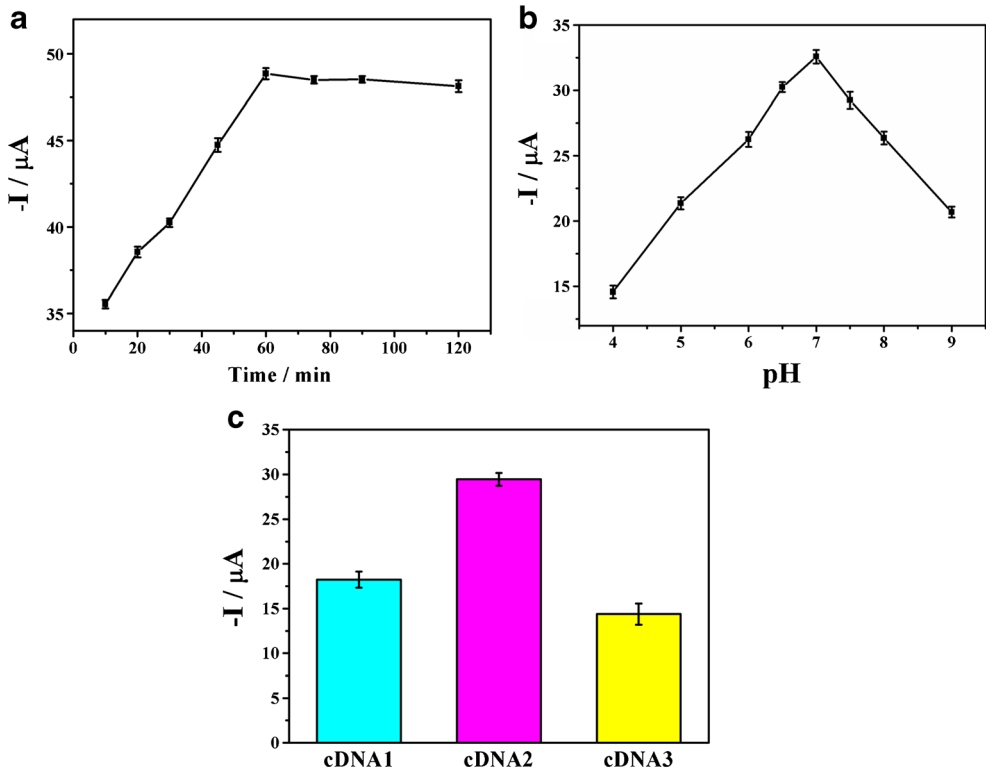

Fig. 3 The effect of electrodeposition time (**a**), the pH of the electrolyte (**b**) and the base number of cDNA (**c**) on the DPV response

signal and the logarithm value of TB concentration in the range of 1×10^{-13}–1×10^{-7} M is obtained ($R = 0.994$) (Fig. 4B). The detection limit is 3.53×10^{-14} M (S/$N = 3$). The analytical performance of our biosensor is better than others reported (Table 2) [35–41]. This may be due to the excellent conductivity and good biocompatibility of N- and P-co-doped graphene, and also the stability of T-DNA and the signal amplification of the RCA assay.

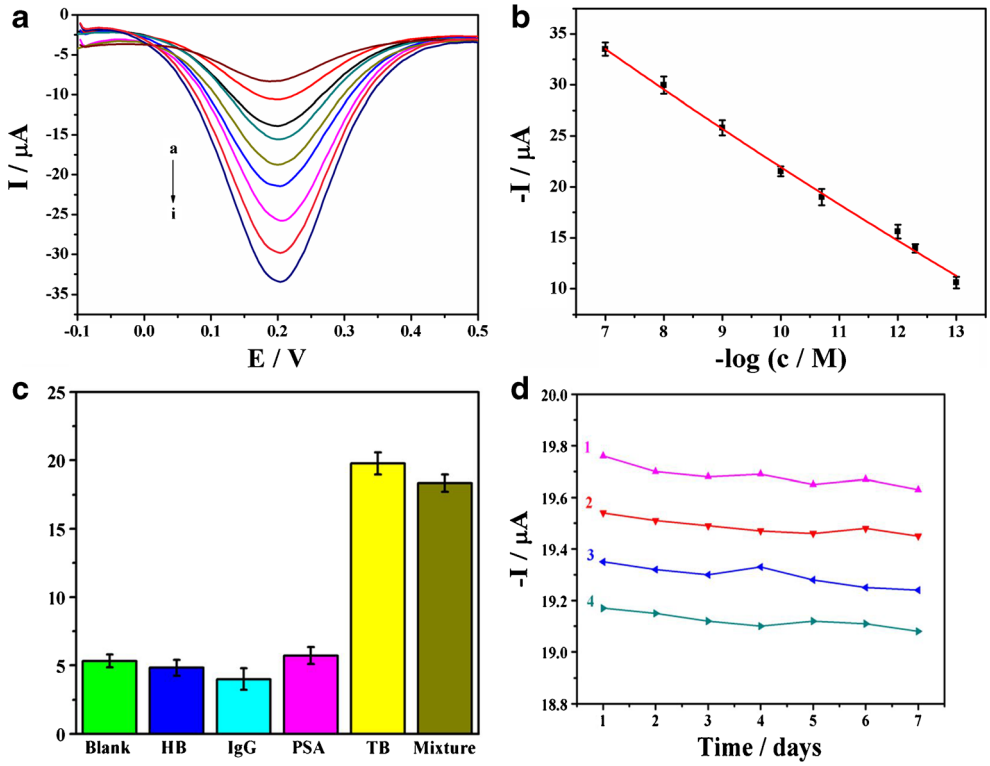

Fig. 4 (**A**) DPVs of TB (**a**–**h**): 0, 0.0001, 0.001, 0.01, 0.1, 1, 10, 100 pmol L^{-1}; (**B**) calibration plots; (**C**) the effect of various compounds; (**D**) the stability

Table 2 The results of TB detection with various methods

Detection method	Linear range (pM)	LOD (pM)	Ref.
Electrochemiluminescence	10–10,000	6.3	[35]
Electrochemical aptasensor	100–25,000	20	[36]
Electrochemical aptasensor	0.3–54	0.14	[37]
Electrochemical aptasensor	10–50,000	5.6	[38]
Electrochemiluminescence	0.4–1000	0.23	[39]
Fluorescence	0.25–25,000	8.9	[40]
Fluorescence	10,000–80,000	1300	[40]
Fluorescence	50–100,000	15	[41]
Electrochemical aptasensor	0.1–100,000	0.035	This work

Selectivity, repeatability and stability

The selectivity of the biosensor was evaluated by mixing 100 pM HB, IgG and PSA into the standard samples. Subsequently, the biosensor was kept in 100 pM TB blended with the above interfering substances. The DPV response changed little compared with pure TB solution (Fig. 4C), demonstrating good selectivity. Three biosensors fabricated with the same method independently were used to determine TB (0.1, 10, 100 pM), and relative standard deviation (RSD) values of 3.21%, 4.82% and 5.15% were obtained, respectively, showing good reproducibility. The stability of the biosensor was also determined. The results in Fig. 4D show that the four biosensors have good stability for storage at 4 °C.

Real sample analysis

The biosensor was used to determine TB in spiked human serum. Different concentrations of TB were mixed with healthy human serum samples obtained from the Affiliated Hospital of Xinyang Normal University, and then detected with the biosensor. The experiment in this work was carried out in compliance with the relevant laws and institutional guidelines, and the study was approved by the Institutional Review Board of the Affiliated Hospital of Xinyang Normal University. Informed consent was also given by every participant. As shown in Table 3, recoveries of 97.0–103.9% with RSDs of 2.9–5.9% were obtained, indicating that the biosensor is feasible for use in real biological samples and has great clinical analysis potential.

Table 3 Recovery tests ($n = 3$)

No.	Added (pM)	Found (pM)	RSDs (%)	Recoveries (%)
1	1	1.02	5.9	102.0
2	20	19.54	4.6	97.7
3	100	103.89	5.3	103.9
4	1000	970.23	2.9	97.0
5	10,000	10,145.4	3.9	101.5

Conclusion

A highly selective and sensitive biosensor for protein detection was fabricated. N- and P-co-doped graphene with good conductivity and large specific surface area was used as electrode supporting substrate. The three-dimensional DNA probe was used to obtain a well-controlled density and minimize nonspecific adsorption, and the RCA signal amplification was applied for a lower detection limit. Under optimal conditions, the biosensor was capable of detecting 3.53×10^{-14} M of TB. The preliminary application of the biosensor was proved by determination of TB in spiked serum samples. The proposed biosensor showed great promise for the sensitive determination of other proteins.

Acknowledgments This work was supported by the National Natural Science Foundation of China (21475115), Henan Provincial Science and Technology Innovation Team (C20150026) and the Nanhu Scholars Program of Xinyang Normal University.

Compliance with ethical standards

Conflict of interest The authors declare no potential conflicts of interest.

References

1. Chen ZQ, Wang C, Hao LJ, Gao R, Li F, Liu SF. Proximity recognition and polymerase-powered DNA walker for one-step and amplified electrochemical protein analysis. Biosens Bioelectron. 2019;128:104–12.
2. Huang KJ, Shuai HL, Zhang JZ. Ultrasensitive sensing platform for platelet-derived growth factor BB detection based on layered molybdenum selenide-graphene composites and Exonuclease III assisted signal amplification. Biosens Bioelectron. 2016;77:69–75.
3. Yao LF, Xu JY, Shi M, Huang Y, Fang LN, Zhao SL, et al. Polydopamine nanoparticle-based multicolor proximity immunoassays for ultrasensitive, multiplexed analysis of proteins using isothermal quadratic amplification. Sensors Actuators B Chem. 2019;282:626–35.
4. Wang YH, Huang KJ, Wu X, Ma YY, Song DL, Du CY, et al. Ultrasensitive supersandwich-type biosensor for enzyme-free amplified microRNA detection based on N-doped graphene/Au nanoparticles and hemin/G-quadruplexes. J Mater Chem B. 2018;6:2134–42.
5. Luo Y, Wang J, Yang LY, Gao T, Pei RJ. In vitro selection of DNA aptamers for the development of fluorescent aptasensor for sarcosine detection. Sensors Actuators B Chem. 2018;276:128–35.
6. Umrao S, Jain V, Anusha Chakraborty B, Roy R. Protein-induced fluorescence enhancement as aptamer sensing mechanism for thrombin detection. Sensors Actuators B Chem. 2018;267:294–301.
7. Chen YX, Huang KJ, He LL, Wang YH. Tetrahedral DNA probe coupling with hybridization chain reaction for competitive thrombin aptasensor. Biosens Bioelectron. 2018;100:274–81.
8. Xu J, Lee ES, Gye MC, Kim YP. Rapid and sensitive determination of bisphenol A using aptamer and split DNAzyme. Chemosphere. 2019;228:110–6.
9. Kim S, Lee S, Lee HJ. An aptamer-aptamer sandwich assay with nanorod-enhanced surface plasmon resonance for attomolar

concentration of norovirus capsid protein. Sensors Actuators B Chem. 2018;273:1029–36.
10. Jarczewska M, Rębiś J, Górski Ł, Malinowska E. Development of DNA aptamer-based sensor for electrochemical detection of C-reactive protein. Talanta. 2018;189(2018):45–54.
11. Wang R, Wang L, Xua XW, Jiang W. An enzyme-free and label-free fluorescence biosensor for microRNA detection based on cascade amplification of DNAzyme-powered three-dimensional DNA walker and hybridization chain reaction. Sensors Actuators B Chem. 2018;268:287–92.
12. Qu XM, Zhu D, Yao GB, Su S, Chao J, Liu HJ, et al. An exonuclease III-powered, on-particle stochastic DNA walker. Angew Chem Int Ed. 2017;56:1855–8.
13. Yuan CJ, Fang J, Duan QY, Yan Q, Guo J, Yuan TX, et al. Two-layer three-dimensional DNA walker with highly integrated entropy-driven and enzyme-powered reactions for HIV detection. Biosens Bioelectron. 2019;133:243–9.
14. Gao Y, Deng XL, Wen W, Zhang XH, Wang SF. Ultrasensitive paper based nucleic acid detection realized by three-dimensional DNA-AuNPs network amplification. Biosens Bioelectron. 2017;92:529–35.
15. Tian R, Ning WH, Chen MH, Zhang C, Li QW, Bai JW. High performance electrochemical biosensor based on 3D nitrogen-doped reduced graphene oxide electrode and tetrahedral DNA nanostructure. Talanta. 2019;194:273–81.
16. Ma JH, Xue L, Zhang ML, Li C, Xiang Y, Liu P, et al. An electrochemical sensor for Oct4 detection in human tissue based on target-induced steric hindrance effect on a tetrahedral DNA nanostructure. Biosens Bioelectron. 2019;127:194–9.
17. Wang YH, Huang KJ, Wu X. Recent advances in transition-metal dichalcogenides based electrochemical biosensors: a review. Biosens Bioelectron. 2017;97:305–16.
18. Li PP, Liu XP, Mao CJ, Jin BK, Zhu JJ. Photoelectrochemical DNA biosensor based on g-C_3N_4/MoS_2 2D/2D heterojunction electrode matrix and co-sensitization amplification with CdSe QDs for the sensitive detection of ssDNA. Anal Chim Acta. 2019;1048:42–9.
19. Urbańczyk E, Maciej A, Stolarczyk A, Basiaga M, Simka W. The electrocatalytic oxidation of urea on nickel-graphene and nickel-graphene oxide composite electrodes. Electrochim Acta. 2019;305:256–63.
20. Qi YL, Cao Y, Meng XT, Cao J, Li XW, Hao QL, et al. Facile synthesis of 3D sulfur/nitrogen co-doped graphene derived from graphene oxide hydrogel and the simultaneous determination of hydroquinone and catechol. Sensors Actuators B Chem. 2019;279:170–6.
21. Zhang J, Yang H, Shen G, Cheng P, Zhang J, Guo S. Reduction of graphene oxide via L-ascorbic acid. Chem Commun. 2010;46:1112–4.
22. El-Gendy DM, Ghany NAA, Allam NK. Green, single-pot synthesis of functionalized Na/N/P co-doped graphene nanosheets for high-performance supercapacitors. J Electroanal Chem. 2019;837:30–8.
23. Zhang XY, Sun SH, Sun XJ, Zhao YR, Chen L, Yang Y, et al. Plasma-induced, nitrogen-doped graphene-based aerogels for high-performance supercapacitors. Light Sci Appl. 2016;5:e16130.
24. Pei W, Zhou S, Bai Y, Zhao J. N-doped graphitic carbon materials hybridized with transition metals (compounds) for hydrogen evolution reaction: understanding the synergistic effect from atomistic level. Carbon. 2018;133:260–6.
25. Zhou J, Wang ZG, Yang DX, Zhang WL, Chen YF. Free-standing S, N co-doped graphene/Ni foam as highly efficient and stable electrocatalyst for oxygen evolution reaction. Electrochim Acta. 2019;317:408–15.
26. Song ZC, Lu XL, Hu Q, Ren J, Zhang WQ, Zheng QJ, et al. Synergistic confining polysulfides by rational design a N/P co-doped carbon as sulfur host and functional interlayer for high-performance lithium-sulfur batteries. J Power Sources. 2019;421:23–31.
27. Zhang L, Zhu G, Zhang C. Homogeneous and label-free detection of microRNAs using bifunctional strand displacement amplification-mediated hyperbranched rolling circle amplification. Anal Chem. 2014;86:6703–9.
28. Torres-Chavolla E, Alocilja EC. Nanoparticle based DNA biosensor for tuberculosis detection using thermophilic helicase-dependent isothermal amplification. Biosens Bioelectron. 2011;26:4614–8.
29. Chen A, Gui G, Zhuo Y, Chai Y, Xiang Y, Yuan R. Signal-off electrochemiluminescence biosensor based on Phi29 DNA polymerase mediated strand displacement amplification for microRNA detection. Anal Chem. 2015;87:6328–34.
30. Tortajada-Genaro LA, Yamanaka ES, Maquieira Á. Consumer electronics devices for DNA genotyping based on loop-mediated isothermal amplification and array hybridisation. Talanta. 2019;198:424–31.
31. Jia YJ, Sun FF, Na N, Ouyang J. Detection of p53 DNA using commercially available personal glucose meters based on rolling circle amplification coupled with nicking enzyme signal amplification. Anal Chim Acta. 2019;1060:64–70.
32. Shuai HL, Wu X, Huang KJ. Molybdenum disulfide sphere-based electrochemical aptasensors for protein detection. J Mater Chem B. 2017;5:5362–72.
33. Hummers WS. Offeman RE. J Am Chem Soc. 1958;80:1339.
34. Ma XX, He XQ. The supporting of $Co_2(OH)PO_4$ onto N, P co-doped graphene via an in-situ hydrothermal assembly synthesis for efficient oxygen reduction reaction. Int J Hydrogen Energ. 2018;43:1415–23.
35. Li YJ, Li YQ, Xu N, Pan JH, Chen TF, Chen YW, et al. Dual-signal amplification strategy for electrochemiluminescence sandwich biosensor for detection of thrombin. Sensors Actuators B Chem. 2017;240:742–8.
36. Zheng YN, Yuan YL, Chai YQ, Yuan R. A label-free electrochemical aptasensor based on the catalysis of manganese porphyrins for detection of thrombin. Biosens Bioelectron. 2015;66:585–9.
37. Wang Y, Zhang Y, Yan T, Fan DW, Du B, Ma HM, et al. Ultrasensitive electrochemical aptasensor for the detection of thrombin based on dual signal amplification strategy of au@GS and DNA-CoPd NPs conjugates. Biosens Bioelectron. 2016;80:640–6.
38. Yang JM, Dou BT, Yuan R, Xiang Y. Proximity binding and metal ion-dependent DNAzyme cyclic amplification-integrated aptasensor for label-free and sensitive electrochemical detection of thrombin. Anal Chem. 2016;88:8218–23.
39. Wang XY, Sun DP, Tong YL, Zhong YS, Chen ZG. A voltammetric aptamer-based thrombin biosensor exploiting signal amplification via synergetic catalysis by DNAzyme and enzyme decorated AuPd nanoparticles on a poly (o-phenylenediamine) support. Microchim Acta. 2017;184:1791–9.
40. Cao Y, Wang ZH, Cao JP, Mao XX, Chen GF, Zhao J. A general protein aptasensing strategy based on untemplated nucleic acid elongation and the use of fluorescent copper nanoparticles: application to the detection of thrombin and the vascular endothelial growth factor. Microchim Acta. 2017;184:3697–704.
41. He JC, Li GK, Hu YL. Aptamer-involved fluorescence amplification strategy facilitated by directional enzymatic hydrolysis for bioassays based on a metal-organic framework platform: highly selective and sensitive determination of thrombin and oxytetracycline. Microchim Acta. 2017;184:2365–73.